2.4 CHARACTERIZATION OF FE THIN FILMS ON {100} ORIENTED $Y_2Ti_2O_7$ SUBSTRATES—T. Stan, Y. Wu, G.R. Odette (University of California Santa Barbara), and H.D. Zhou (University of Tennessee)

OBJECTIVE

The objective of this work is to gain insight into the oxide-matrix interfaces found in Nanostructured Ferritic Alloys by studying the meso-scale Fe - {100} oriented $Y_2Ti_2O_7$ substrate bilayers.

SUMMARY

Nanostructured Ferritic Alloys (NFAs), a variant of oxide dispersion strengthened steels, contain a high density (≈ $5x10^{23}/m^3$) of ≈ 2.5 nm average diameter Y-Ti-O nano-oxides (NOs) which help impede dislocation climb and glide, stabilize dislocation and grain structures, and trap He in fine-scale bubbles at matrix-NO interfaces. To complement other studies of the NOs themselves, mesoscopic-scale bilayer interfaces were fabricated by electron beam deposition of a thin Fe film on a {100} $Y_2Ti_2O_7$ (YTO) bulk single crystal substrate. These bilayers were prepared for He implantation and charged particle irradiations to experimentally observe defect interface interactions and the partitioning of He between the Fe, YTO, and the associated interface. We report, for the first time, the dominant epitaxial orientation relationship (OR) for a polycrystalline Fe film on {100} YTO: $\{110\}_{Fe}\backslash\backslash\{100\}_{YTO}$ and $<100>_{Fe}\backslash\backslash<110>_{YTO}$. One large grain region had an OR that is also found in embedded NOs: $\{100\}_{Fe}\backslash\backslash\{100\}_{YTO}$ and $<100>_{Fe}\backslash\backslash<110>_{YTO}$. HRTEM studies show clean semicoherent interfaces, with misfit dislocation spacings consistent with the calculated near coincidence site lattices.

PROGRESS AND STATUS

Introduction

Materials for nuclear fusion applications must reliably perform at high temperatures and accommodate high levels of helium (He) and displacement damage. Nanostructured Ferritic Alloys (NFAs) are a promising class of Fe-Cr-based stainless steels with outstanding mechanical properties, are thermally stable up to 950°C, and are remarkably irradiation tolerant [1–4]. NFAs contain a high density of N ≈ $5x10^{23}/m^2$ of YTO nano-oxides with an average diameter of <d> ≈ 2.5 nm. The NOs impede dislocation climb and glide, stabilize dislocation and fine grain structures, and most notably, trap He in fine-scale bubbles at the matrix-NO interfaces. The high density of bubbles prevents the formation of growing voids and He accumulation at grain boundaries, which would otherwise degrade the dimensional stability, creep and fracture properties of most structural alloys, as is the case for conventional 9 Cr tempered martensitic steels. He bubbles also act as recombination sites for vacancies and self-interstitials, thus promoting radiation damage self-healing.

Research to characterize NO compositions, structures, misfit strains, core shell structures, interface characteristics, and NO-matrix orientation relationships (ORs) is continuing [5–8]. Most of the smallest NOs are the $Y_2Ti_2O_7$ (YTO) fcc pyrochlore phase [7–15]. Detailed characterization and analysis of the NO-matrix interfaces is needed to develop first principles and atomic-scale models that are part of multi-scale efforts to guide the selection of processing paths and to predict the behavior of NFAs and NOs in irradiation service environments. YTO-matrix ORs are of particular interest, because they impact the selection of compositions and processing paths, service stability, mechanical properties and irradiation tolerance of NFAs. Important interface characteristics include their structures, chemistries, defects, misfit strains, free energies and, perhaps most importantly, NO interactions with He. The embedded NOs and their interfaces are challenging to characterize, partly due to their small nm-scale size.

A comprehensive first principles study by Jiang et al. [16–18] showed that He is deeply trapped in the YTO NOs at an energy of ~1.4 eV lower than in the Fe-Cr matrix. Coupled with the ultra high NO sink strength, this ensures that the eventual fate of He is to reside in nm-scale bubbles on the oxide interfaces. The sequence of events is as follows. First He migrates to, and is deeply trapped in, the NOs. However, the He energy is even lower in sufficiently sized NO-matrix interface bubbles, that quickly nucleate and

grow, thereby draining the He from the NOs. Thus characterization of the matrix-NO-interface He partitioning is critically important and is one of the major goals of the experiment described below.

To study the He transport and fate in a controlled fashion, our approach was to deposit Fe on oriented YTO single crystal substrates to create bilayers with mesoscopic-scale interfaces that facilitate detailed characterization studies. Ideally, the bilayer interfaces are the same, or similar to, those found in the embedded NOs. One such interface was found in the bilayer fabricated here, although another orientation relationship was the dominant naturally selected interface. As well as facilitating He and point defect transport and fate studies, characterization of the Fe-YTO interfaces will provide input to first principles interface modeling.

We previously reported a study of Fe deposited on {111}YTO [19]. However, {111}YTO interfaces are not usually observed in the embedded NOs. The following results are for Fe depositions on {100}YTO substrates are a significant extension of previous research. The naturally selected bilayer interfaces were characterized and compared to NOs in NFAs.

Experimental Procedure

The details of sample fabrication and characterization techniques are covered in a previous publication [19]. The feed rods for the YTO single crystal growth were prepared by solid state reactions. Appropriate mixtures of Y_2O_3 and TiO_2 were ground together, and pressed into 6 mm diameter, 60 mm long, rods under a 400 atm hydrostatic pressure, followed by calcinations in air at 1673 K (1400°C) for 24 hrs. The Czochralski growth was carried out in 5 atm oxygen in an IR-heated image furnace (NEC) at a rate of 3 mm/hr. The YTO single crystals were oriented with a {100} surface and corresponding 2 mm thick wafers were cut from the rod using a wire saw.

An Allied Multiprep was used to polish the wafers using a sequence of diamond lapping films, followed by a final 15 minute polishing step using a 0.02 µm non-crystallizing colloidal silica suspension. The substrates were then placed in an ultrasonic bath with 90% reverse osmosis water and 10% Micro-Organic soap. This was followed by an acetone ultrasonic bath for 10 minutes, and finally an isopropanol ultrasonic bath for 10 minutes.

The YTO single crystal wafer was loaded into an electron beam deposition system and heated to 1073 K (800°C) at a rate of 0.166 K/s. After outgassing for 1 h, 2 µm of Fe was deposited at a rate of ~8 nm/s (250 s total) at chamber pressure of 3 x 10^{-6} torr. After deposition the Fe-YTO bilayer was annealed in vacuum at 1073 K (800°C) for 30 min. The Fe-{100}YTO substrate bilayer was slowly cooled to room temperature prior to unloading.

Electron backscatter diffraction (EBSD) pole figures, orientation maps, and 3D representations were obtained using a FEI Quanta 400F field-emission scanning electron microscope (SEM). A FEI HELIOS Focus Ion Beam (FIB) tool was used to first deposit ~1 µm of protective platinum over areas of interest. <30 nm thick lift-outs of the Fe-YTO interface were extracted, and a low energy 2 keV 5.5 pÅ gallium beam was used for the final cleaning. Hig-resolution transmission electron microscopy (HRTEM), scanning TEM (STEM), and energy dispersive xray (EDX) observations were carried out on a 300 keV FEI Titan TEM. CrystalMaker software was used to analyze the bulk lattice matching.

Results

<u>SEM and EBSD Characterization</u>

The 2 µm thick Fe film had two dominant morphologies: a larger {110}Fe polycrystalline region covering ~99% of the deposit, and a smaller (100 µm x 100 µm) {100}Fe monocrystalline grain. The monocrystalline grain is of particular interest because it has an OR found in embedded NOs (as discussed below). The multipart Figure 1 and Figure 2 show Scanning Electron Microscopy (SEM) and Electron Backscatter Diffraction (EBSD) data from the two films. Note the figures are equally scaled and formatted to facilitate side-by-side comparisons.

Figure 1 shows SEM and EBSD data from the polycrystalline side. Figure 1a is a SEM image showing that the polycrystalline Fe layer is comprised of 1 – 3 µm grains. Ledges are seen on the surface of some grains. The EBSD inverse pole figure (IPF) map in Figure 1(b) shows a strong {110} out-of-plane orientation. The dark areas are locations where the electron backscattered diffraction pattern could not be indexed, often at grain boundaries. Figure 1c shows the same EBSD data as Figure 1b, but represented as an Euler pole figure (PF) map where each full crystallographic orientation is assigned a unique color. The grains all have a {110} out-of-plane orientation and four in-plane orientations represented by various colors. Comparing the SEM image in Figure 1a and the Euler map in Figure 1c, shows that the green and orange variants coalesce, as do the purple and blue grains.

Figure 1d shows three PFs (<100>, <110> and <111> reflections) for the same data as Figure 1b, colored according to the out-of-plane grain orientation (IPFZ). For clarity, only reflections from the grain centers are shown in the PFs. Spots are only seen in the center of the <110> PF, confirming the strong {110} Fe texturing. Figure 1e again shows three PFs, but colored according to the Euler orientations. The four grain variants are clearly separated into four orientations (purple, blue, green and orange). Figure 1f shows the PFs for the YTO substrate with a <100> spot close to the center reflecting the {100} YTO surface orientation.

The Fe-YTO orientation relationship (OR) was obtained by matching spots in the Fe PFs in Figure 1(e) with the accompanying YTO PFs in Figure 1f. The overlapping center spots from the <110>Fe PF and the <100>YTO PF indicate parallel surfaces. Similarly, the overlapping spots at the PF rims indicate parallel in-plane directions. Thus, the OR for the polycrystalline film is:

$\{110\}_{Fe}\backslash\backslash\{100\}_{YTO}$ and $<111>_{Fe}\backslash\backslash<110>_{YTO}$

This edge-on-cube orientation has not been observed for embedded NOs in NFAs. The 3-dimensional renderings in Figure 1g show that the four Fe grain variants have a <111> Fe direction matched with one of the two <110> YTO in-plane directions. The purple and blue grains share a common <111> Fe direction, as do the green and orange grains. The purple/blue and green/orange grain pairs have the exact same OR with the substrate, but are 90° rotated from one another to match the 2-fold symmetry of the underlying {100} YTO.

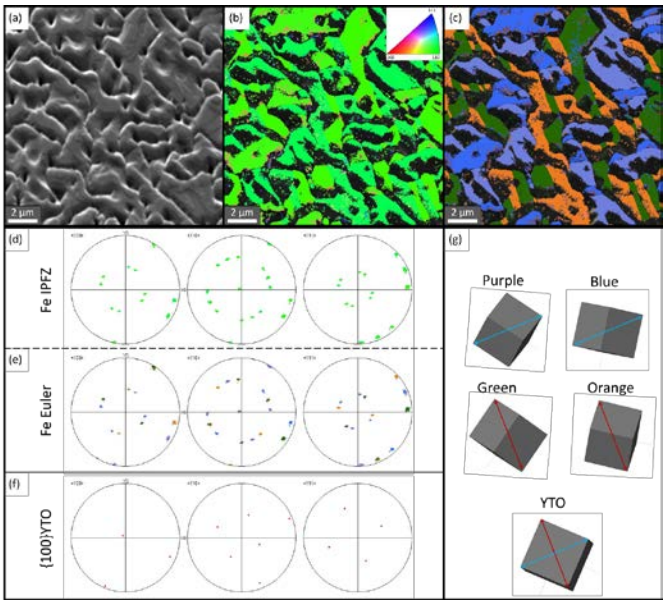

Figure 1. SEM/EBSD data from polycrystalline side showing (a) SEM image of 1 – 3 micron elongated grains, (b) IPFZ map with out-of plane {110} Fe texturing, (c) Euler map indicating four in-plane variants, (d) IPFZ pole figures, (e) Euler pole figures, (f) YTO pole figures, (g) 3D representation of {110} Fe grains and {100} YTO substrate.

Figure 2 shows SEM and EBSD data from the 100 µm x 100 µm monocrystalline grain. Figure 2a is an SEM image showing one continuous flat film with no grain boundaries. Surface ledges are seen on the film surface. Figure 2b shows an EBSD inverse pole figure (IPF) map of the same area as Figure 2a, indicating the out-of-plane {100} Fe crystallographic texturing. The black streaks coincide with ledges where the EBSD signal could not be indexed. Figure 2c represents the same EBSD data as Figure 2b but as an Euler PF map showing only one in-plane orientation.

Figure 2d shows three PFs (<100>, <110> and <111> reflections) for the same data that is in Figure 2b, with a strong, uniformly red out-of-plane {100} grain texturing. Figure 2e shows three PFs, all having same color associated with only one in-plane orientation. Figure 2f repeats the illustration in Figure 1f for easy comparison. The Fe-YTO OR for the monocrystalline film was obtained by matching spots in the Fe PFs in Figure 2e with the accompanying YTO PFs in Figure 2f. The OR for the monocrystalline crystalline film is close to:

$\{100\}_{Fe}\backslash\backslash\{100\}_{YTO}$ and $\langle 100\rangle_{Fe}\backslash\backslash\langle 110\rangle_{YTO}$

This type of edge-on-cube orientation has been observed for NOs in NFAs [8]. The 3D renderings in Figure 2g confirm that there is only one epitaxial orientation relationship between the Fe film and the underlying YTO substrate.

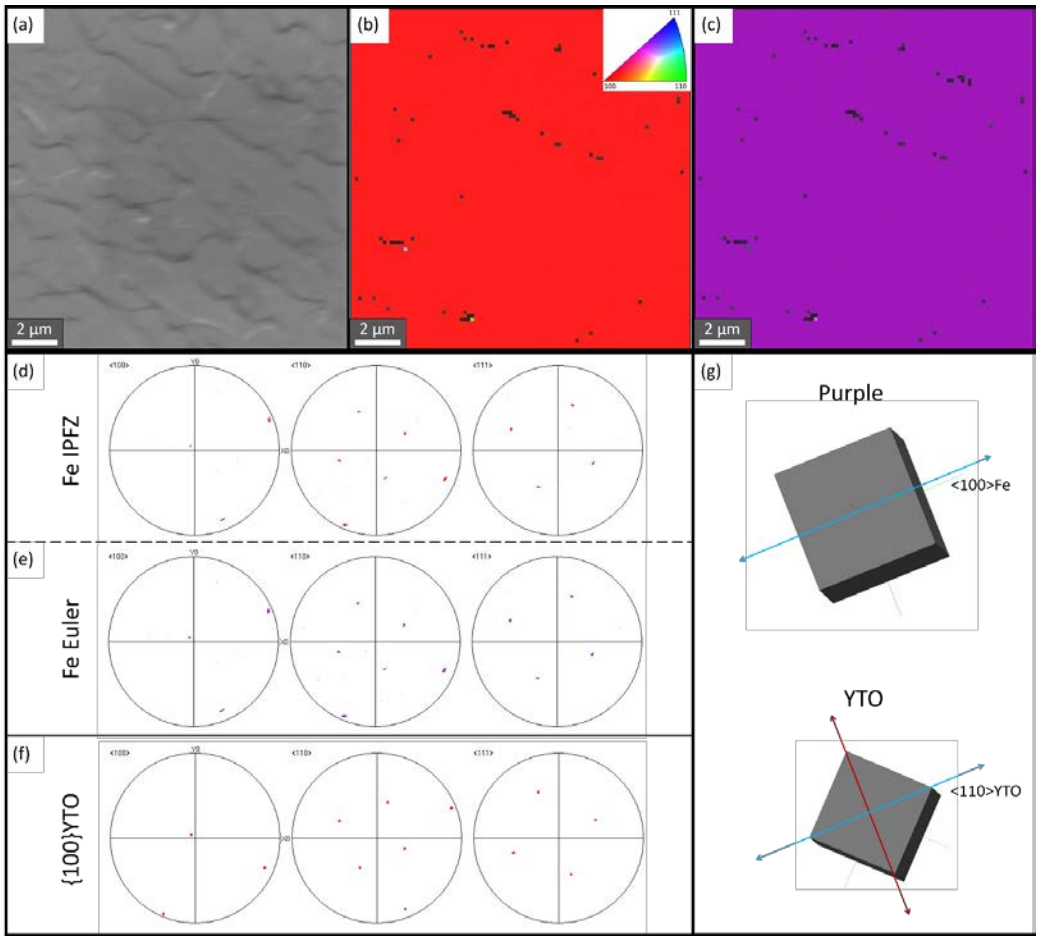

Figure 2. SEM/EBSD data from monocrystalline side showing (a) SEM scan showing a large flat area, (b) IPFZ map showing out-of plane {100} Fe texturing, (c) Euler map indicating one in-plane variant, (d) IPFZ pole figures, (e) Euler pole figures, (f) YTO pole figures, (g) 3D representation of {100} Fe film and {100} YTO substrate.

HRTEM Characterization

High Resolution Transmission Electron Microscopy (HRTEM) was used to investigate the structure of the Fe-YTO interfaces. Figure 3 shows HRTEM images from: (a) one of the {110} Fe polycrystalline grains; and, (c) the large monocrystalline grain. In both cases, the images are aligned with the <110> YTO in-plane zone axis, with the {100} YTO surface pointing up. The figures are equally scaled and formatted to facilitate side-by-side comparisons.

Figure 3a shows that the <111> Fe and <110> YTO in-plane zone axis directions are aligned and the corresponding planes are well resolved. The white arrows indicate the location of periodic interfacial misfit dislocations which are ~ 0.7 nm apart. These are more easily seen in the Fast Fourier Transform (FFT) image in Figure 3b. Energy dispersive x-ray (EDX) scans (not shown) indicate that Fe and YTO are not intermixed at the interface, and are free of detectible contaminants.

Figure 3c shows corresponding monocrystalline {100} Fe interface. There is a slight (~5°) misalignment between the <100> Fe and <110> YTO zone axis thus the YTO lattice is not resolved in the image. The

white arrows indicate the location of periodic misfit dislocations that are ~1.4 nm apart. Notably, this is twice the spacing found for the polycrystalline portion in Figure 3a. EDX and preliminary atom probe tomography studies (not shown) indicate clean interfaces without a contaminant interfacial layer.

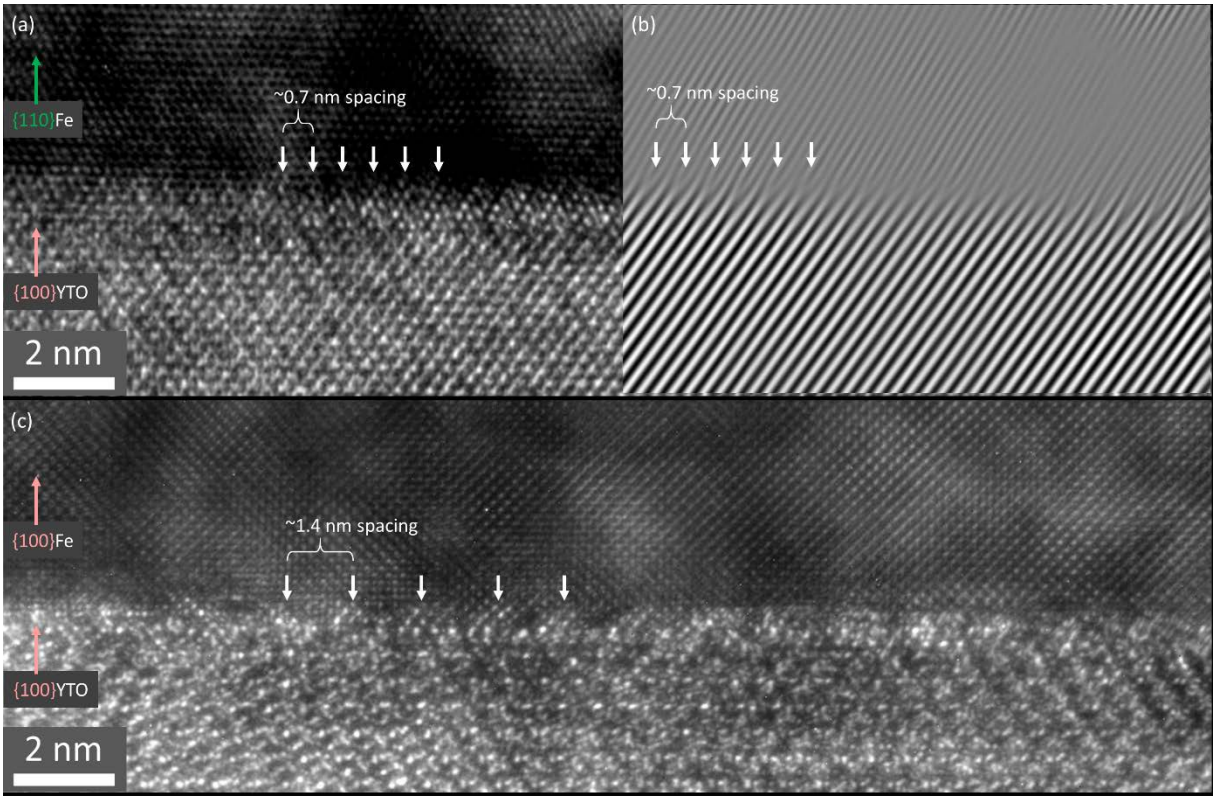

Figure 3. HRTEM image from (a) the polycrystalline side, (b) the Fast Fourier Transform, and (c) the monocrystalline side. Misfit dislocations are shown with white arrows.

For the Fe deposition conditions in this study, two epitaxial ORs were observed. The majority of the film was composed of 1 – 3 µm grains with: $\{110\}_{Fe}\backslash\backslash\{100\}_{YTO}$ and $<111>_{Fe}\backslash\backslash<110>_{YTO}$. However, a large 100 µm x 100 µm grain had an OR found in embedded NOs: $\{100\}_{Fe}\backslash\backslash\{100\}_{YTO}$ and $<100>_{Fe}\backslash\backslash<100>_{YTO}$.

CrystalMaker was used to analyze the lattice matching of the two interfaces observed in this study. Figure 4a shows a top-view of the lattice matching from the polycrystalline side. Fe atoms are orange, Y green, Ti blue, and O red. Along the $<111>_{Fe}\backslash\backslash<110>_{YTO}$ direction, every tenth d_{222} Fe plane has a coincident match with every fourth d_{440} YTO plane. The resulting misfit dislocation spacing is 0.71 nm. Along the $<112>_{Fe}\backslash\backslash<110>_{YTO}$ direction, every six d_{112} Fe plane has a coincident match with every fourth d_{440} YTO plane. The resulting misfit dislocation spacing is also 0.71 nm. The near coincidence site lattice (NCSL) is a 0.71 nm x 0.71 nm square, shown as a black dotted line in Figure 4a, that matches the HRTEM observations in Figure 3a. The small dislocation spacing indicates a higher energy semicoherent interface.

Figure 4b shows the CrystalMaker monocrystalline interface. In this case, with only in-plane $<100>_{Fe}\backslash\backslash<100>_{YTO}$ directions, every fifth d_{100} Fe plane has a coincident match with every fourth d_{440} YTO plane. This would seem to imply a misfit dislocation spacing and NCSL of 0.71 nm, the same as for the polycrystalline grain. However, analysis of the atom matching in Figure 4b shows that the 0.71 nm NCSL would not lead to a periodic lattice. Twice this distance is required, thus the actual expected misfit dislocation spacing is 1.43 nm. The resulting NCSL size is a 1.43 nm x 1.43 nm square that also matches

the HRTEM observations in Figure 3b. The lower dislocation density implies a lower energy semicoherent interface.

It is not yet clear why two Fe orientations were observed. In previous studies of Fe depositions on {111} YTO [19], a dominant {110} Fe texturing was observed for grains with clean Fe-YTO interfaces. However, Fe grains had a {100} orientation when a 2 - 3 nm thick contaminant interlayer was present at the Fe-YTO interface. In the present study, neither the polycrystalline side nor the monocrystalline grain had an observable interlayer. It is possible that grain island nucleation events take place at locally contaminated or otherwise defected sites. Note that rapid, highly driven, self selection of interfaces may not always follow the minimum energy path. Local contamination or defect sites would be very difficult to detect by the HRTEM, EDX, and APT characterizations tools used in this study. However, the two {100}YTO interface variants actually present an opportunity to examine the similarities and differences in future He implantation experiments.

Even for cases with the same general OR, there are differences between the interfaces of the NOs embedded in NFAs versus the Fe-YTO bilayers in this study. The smallest NOs are likely coherent, with misfit strains partitioned between the Fe and YTO precipitate that increase with decreasing size. For example, a 2 nm x 3 nm YTO NO had ~5% coherency strain with a 5 x 7 NCSL [8]. Embedded NOs typically also have core-shell structures [5–7]. In contrast, the meso-scale bilayer interfaces are semicoherent with ORs differ from those most frequently found for embedded NOs.

We have also completed Fe depositions on {110} YTO using molecular beam epitaxy. Preliminary results show the Fe films have an axiotaxial OR that is close to: $\{100\}_{Fe}\backslash\backslash\{110\}_{YTO}$ and $<100>_{Fe}\backslash\backslash<100>_{YTO}$. However, details of this deposition and interactions with He will be the subject of a future publication. All three Fe - {100}, {110}, and {111} YTO bilayers will be subject to high temperature He implantations and charged particle irradiations of the Fe layer. The simplified bilayer model system of Fe on YTO provides the opportunities to use bulk mass spectroscopy measurements of the (Fe+YTO) and (YTO only) to observe the He partitioning. The corresponding He bubble size distributions, number densities, volume fractions, and spatial distribution will be observed using TEM. These experimental observations are critical to calibrating models that predict the behavior of NFAs and NOs in irradiation environments.

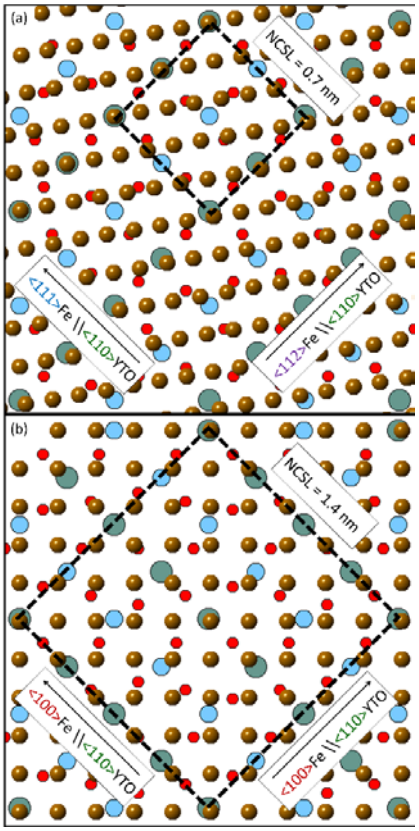

Figure 4. CrystalMaker renderings of the Fe-YTO interfaces from the (a) polycrystalline side and (b) monocrystalline side. Fe is shown in orange, Y in green, Ti in blue, and O in red. The black dotted lines show the near-coincidence site lattices.

Summary and Future Studies

Mesoscopic epitaxial Fe-YTO bilayers were successfully fabricated by electron beam Fe on {100} YTO single crystal surfaces. We report for the first time, the dominant fine grained polycrystalline OR is $\{110\}_{Fe}\backslash\backslash\{100\}_{YTO}$ and $<111>_{Fe}\backslash\backslash<110>_{YTO}$ with four variants that match the underlying substrate symmetry. HRTEM showed a semicoherent interface with misfit dislocation spacing of ~ 0.7 nm, consistent with CrystalMaker analysis. In contrast, a larger monocrystalline Fe grain had a $\{100\}_{Fe}\backslash\backslash\{100\}_{YTO}$ and $<100>_{Fe}\backslash\backslash<110>_{YTO}$ OR that is also found in embedded NOs. HRTEM showed a semicoherent monocrystalline bilayer interface with misfit dislocation spacing of ~ 1.4 nm. Unlike the monocrystalline grain, which was only observed on one bilayer sample, the polycrystalline OR is highly reproducible in electron beam deposition of Fe on {100} YTO.

Finally, we note that the bilayers were prepared for future He implantations and charged particle irradiations, with one objective being to experimentally observe the partitioning of He between the Fe, YTO, and associated interface. These studies will be used to inform multiscale models to predict NFA performance in fusion and fission reactor environments.

Acknowledgements

The authors thank D. Stave, G. Seward, P. Wells (UCSB) for help with various parts of the data acquisition and analysis. We thank Professor Y. Jiang at the Central South University in China for many helpful discussions and providing key insights on interfaces in a collaboration partially supported by NSF of China 51471189. Crystal growth was supported by NSF DMR 1350002. The characterization was done at the UCSB CNSI Microstructure and Microanalysis Facility: an NSF MRSEC, supported by NSF DMR 1121053. This work was supported by the U. S. Department of Energy, Office of Fusion Energy Sciences, under grant DE-FG03-94ER54275.

References

[1] G. R. Odette: *JOM*, 2014, vol. 66, p. 2427.
[2] G.R. Odette, M.J. Alinger, and B.D. Wirth: *Annu. Rev. Mater. Res.*, 2008, vol. 38, pp. 471–503.
[3] N. Cunningham, Y. Wu, D. Klingensmith, et al.: *Mater. Sci. Eng. A*, 2014, vol. 613, pp. 296–305.
[4] Y. Dai, G. R. Odette, and T. Yamamoto: *The Effects of Helium in Irradiated Structural Alloys*, 1st ed., Elsevier Inc., 2012.
[5] Emmanuelle A. Marquis: *Appl. Phys. Lett.*, 2008, vol. 93, pp. 10–13.
[6] S. Liu, G.R. Odette, and C.U. Segre: *J. Nucl. Mater.*, 2014, vol. 445, pp. 50–56.
[7] V. Badjeck, M.G. Walls, L. Chaffron, et al.: *J. Nucl. Mater.*, 2015, vol. 456, pp. 292–301.
[8] Yuan Wu, Jim Ciston, Stephan Kräemer, et al.: *Acta Mater.*, 2016, vol. 111, pp. 108–15.
[9] J. Ribis and Y. De Carlan: *Acta Mater.*, 2012, vol. 60, pp. 238–52.
[10] J. Ribis and S. Lozano-Perez: *J. Nucl. Mater.*, 2014, vol. 444, pp. 314–22.
[11] Karl Dawson and Gordon J. Tatlock: *J. Nucl. Mater.*, 2014, vol. 444, pp. 252–60.
[12] M. Tamura, H. Sakasegawa, K. Shiba, et al.: *Metall. Mater. Trans. A*, 2011, vol. 42, pp. 2176–88.
[13] Y. Wu, E. M. Haney, N. J. Cunningham, et al.: *Acta Mater.*, 2012, vol. 60, pp. 3456–68.
[14] A. J. London, B. K. Panigrahi, C. C. Tang, et al.: *Scr. Mater.*, 2016, vol. 110, pp. 24–27.
[15] R. Kasada, N. Toda, K. Yutani, et al.: *J. Nucl. Mater.*, 2007, vol. 367-370 A, pp. 222–28.
[16] Litong Yang, Yong Jiang, G. Robert Odette, et al.: *Acta Mater.*, 2013, vol. 61, pp. 7260–70.
[17] Litong Yang, Yong Jiang, G. Robert Odette, et al.: *J. Appl. Phys.*, 2014, vol. 115, p. 143508.
[18] Litong Yang, Yong Jiang, Yuan Wu, et al.: *Acta Mater.*, 2016, vol. 103, pp. 474–82.
[19] Tiberiu Stan, Yuan Wu, George R. Odette, et al.: *Metall. Mater. Trans. A Phys. Metall. Mater. Sci.*, 2013, vol. 44, pp. 4505–12.